



Design and Hydrodynamic Analysis of Buoy Structure with Dynamic Vibration Absorber System

Mohamad Luthfi Ramadiansyah^{1, a)}, Edwar Yazid^{1, b)}, Budi Azhari^{1, c)}, Rahmat^{1, d)}, Muhammad Fathul Hikmawan^{1, e)}, and Aditya Sukma Nugraha^{1, f)}

¹Research Center for Smart Mechatronics, National Research and Innovation Agency (BRIN), KST Samaun Samadikun, Bandung, Indonesia.

Corresponding Author's email: moha057@brin.go.id

Abstract. Ocean wave excitation contributes to the emergence of noise in the communication system that is applied to the ocean. This paper delivers the preliminary design of the smart buoy with noise reduction capability provided by the attached dynamic vibration absorber (DVA) automation system. Hydrostatic stability and hydrodynamic characteristic of the designed buoy structure are two main objectives in this study by generating numerical calculations using ANSYS AQWA in the irregular wave condition and variations in mooring line types. Finding result shows that the designed buoy structure is in stable equilibrium with a metacentric height of 0.456 m and has the highest amplitude response of 0.4 Hz for 6 DoF (Degrees of Freedom) of the buoy motion. The four-lines catenary mooring has delivered a good performance in the hydrodynamic time response analysis compared to the single-taut and single-line catenary moorings by producing the smallest buoy displacement with a maximum surge of 3.354 m, sway 0.287 m, heave 1.874 m, roll 22.818°, pitch 24.427°, and yaw 54.542°, and smallest cable tension with a maximum value of 32.175 kN. This study can be used to develop a DVA automation system and be extended by experimental validation.

Keywords: Buoy design, Hydrostatic stability, Hydrodynamic characteristic, Waves excitation, Mooring lines.

1 INTRODUCTION

Telecommunication and navigation systems development currently keeps growing and expanding, not only for its receiving and transmitting signal technology but also in terms of the geographic aspect of its application. Ocean, as the most area of the earth's surface approximately 70% [1], has been observed for some applications that use telecommunication systems in their operation, such as tsunami early warning systems [2], ocean environment observation [3,4], ship navigation [5], and communication transmitter at the middle of the sea [6]. The system should be maintained its position to keep above the water surface and not sweep away by the ocean waves on a floating structure that widely uses a moored buoy. It was used in the Indonesian sea for navigation, research of water contamination by PLUTO [7], and a tsunami early warning system by Ina-TEWS that use a GPS system [8]. Data acquisition on offshore

operations is habitually held in a real-time condition [9], making system reliability and accuracy an essential consideration. With the floating condition, the attitude keeps changing as long as the ocean waves appear. It can generate noise in the data acquisition process by an applied sensor and makes lower accuracy data [10, 11]. Research by Schone et al. [8] show the water level measurement result on GITEWS has found a lot of noise that cannot be solved. Wang et al. [12] also found data bias in the acquisition process in high-frequency ocean waves. In the radio transponder application, noise can make ground-based radar receives shifted frequency [13]. Therefore, designing a buoy structure for a communication system that can reduce noise due to ocean waves, particularly in the Indonesian Sea is important. This research is working on the design and hydrodynamic analysis of the moored buoy with a dynamic vibration absorber system for communication noise reducer applications with a numerical approach to defining hydrodynamic characteristics in random wave conditions using the commercial software ANSYS AQWA. This software is generally used by many researchers in the hydrodynamic analysis of floating structures for wave energy converters (WEC) [14, 15], wind turbines [16, 17], and breakwaters [18, 19]. This approach obviously can reduce research costs compared to the experimental method to obtain the optimum design and has advantages to be applied in the various environmental condition, easy for geometry and configuration adjustment, and more efficient in the time spent. This research selects two types of mooring methods for analysis with different types of cable materials. The determination of buoy geometry parameters also will be discussed in this research using analytical calculation.

2 DESIGN DESCRIPTION

Buoy geometry was designed as illustrated in Fig. 1, which consists of five sections, such as the floater, frame, top plate, dynamic vibration absorber (DVA) system, and tower. The shape of some sections was built similarly to the existing buoy, and the prior novel of this design in the DVA system. This system can absorb buoy displacement caused by ocean waves subjected to the electronic component box where the communication sensor will be installed and be expected to reduce the noise. This study's scope is limited to determining geometry parameters, simulation of the mooring buoy, and analysis of its hydrodynamic characteristics to ascertain design stabilization when applied to the ocean in the 3 types of mooring systems that are shown in Fig. 2. Single-taut mooring has linear stiffness characteristic that usually used on the shallow water [20]. The single-line catenary mooring consists of two materials, chain and wire rope, with higher durability and lower maintenance cost. The four-lines catenary mooring has similar material to the single-line type with four positions of moored and anchor which is more safety for operation. It has been determined that the ocean depth in this study will be operated at 50 m depth and working on the irregular wave which has 2 m of specific wave height.

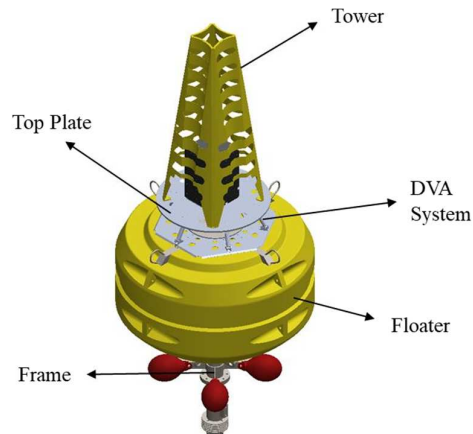


Fig. 1. Construction of Buoy with DVA System.

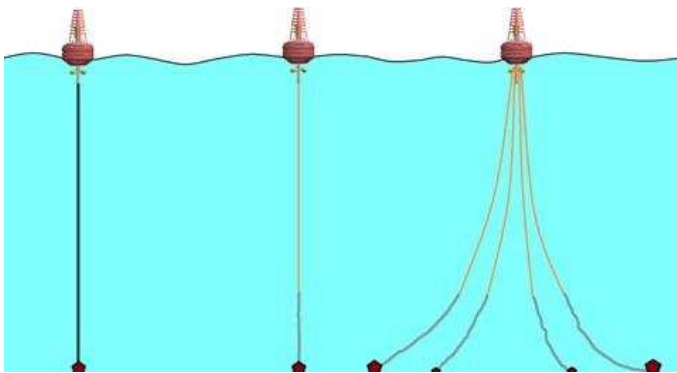


Fig. 2. Mooring Type: Taut (Left), Single-line Catenary (Middle), Four-lines Catenary (Right).

3 MATHEMATICAL MODEL

The mooring buoy is simulated by using the numerical BEM (boundary element method) in the commercial software ANSYS Aqwa. To analyze the hydrodynamic characteristic of the buoy, some mathematical models are used to obtain some geometry parameters and as a basis of the BEM in this simulation.

3.1 Geometry Parameters

The center of gravity is an essential parameter for the stability analysis of a floating structure that corresponds to the center of buoyancy. Analytically, it can be calculated by using (1), which corresponds to the average of component weights multiplied by their distances from a reference point.

$$CoG = \frac{\sum_{i=1}^N W_i r_i}{W_{tot}} \tag{1}$$

Terms CoG is center of gravity position at three axes (x, y, z) in m, W_i is weight of each component in N, r_i is center of gravity of each component in m, and W_{tot} is the total weight of structural system in N. Afterward, mass moment of inertia of the buoy system can be defined by following (2) below :

$$I = \int_m r_{cm}^2 dm \tag{2}$$

Terms I is mass moment of inertia in $kg.m^2$ and r_{cm} is center of mass position in m. To simplify calculation and simulation, it can be expressed in each axis that follows (3).

$$I_{xx} = \int_m (y^2 + z^2) dm, \quad I_{yy} = \int_m (x^2 + z^2) dm, \quad I_{zz} = \int_m (x^2 + y^2) dm \tag{3}$$

In hydrostatic stability, one of the criteria for a free-floating body is the metacentric height, \overline{GM} . A stable equilibrium is defined by a value of $\overline{GM} > 0$, neutral when $\overline{GM} = 0$ and unstable equilibrium if $\overline{GM} < 0$. Longitudinal and transverse metacentric heights are defined as (4).

$$\overline{GM}_L = \frac{I_{YY}}{\nabla}, \quad \overline{GM}_T = \frac{I_{XX}}{\nabla} \tag{4}$$

Terms \overline{GM}_L and \overline{GM}_T are longitudinal and transverse metacentric height in m, ∇ is water volume displacement in m^3 , I_{XX} and I_{YY} are respectively the second moments of the cut water-plane area about the center of buoyancy at x and y axis in m^4 which are defined as (5).

$$I_{XX} = \int_A (y - y_b)^2 dA, \quad I_{YY} = \int_A (x - x_b)^2 dA \tag{5}$$

Where A is cut water-plane area in m^2 and x_b, y_b are center of buoyancy position in m. Some iterations should be done in determining structural geometry shape and dimension until the system attains stability in hydrostatic equilibrium.

3.2 Ocean Wave Spectrum

Practically, the most common ocean environment has random wave conditions instead of regular waves. The linear theory is used to express the sea waves as the accumulation of numerous wave components as in (6).

$$\zeta(x, y, t) = \sum_{m=1}^{N_d} \sum_{j=1}^{N_m} a_{jm} e^{i(k_{jm}x \cos \chi_m + k_{jm}y \sin \chi_m - \omega_{jm}t + \alpha_{jm})} \tag{6}$$

$$a_{jm} = \sqrt{2S_m(\omega_j) \Delta \omega_j} \tag{7}$$

Terms ζ is the wave elevation in m, N_d and N_m are respectively the number of wave directions and the number of wave components along each wave direction χ_m , α_{jm} is the phase angle of wave component jm , a_{jm} is the wave amplitude in m, ω_{jm} is the wave

frequency in rad/s, k_{jm} is the wave number, and $S_m(\omega)$ is wave spectrum for the m -th sub-directional waves [21]. JONSWAP spectrum is used in this study by reason of the imbalance of energy flow in the wave system can be considered. Its spectral ordinate at a frequency (ω) is defined in (8).

$$S(\omega) = \frac{\alpha g^2 \gamma^a}{\omega^5} \exp\left(-\frac{5\omega_p^4}{4\omega^4}\right) \tag{8}$$

$$a = \exp\left[-\frac{(\omega - \omega_p)^2}{2\sigma^2 \omega_p^2}\right] \tag{9}$$

$$\sigma = \begin{cases} 0.07 & \text{where } \omega \leq \omega_p \\ 0.09 & \text{where } \omega > \omega_p \end{cases} \tag{10}$$

$$\alpha = \left(\frac{H_s}{4}\right)^2 \int_0^\infty \frac{g^2 \gamma^a}{\omega^5} \exp\left(-\frac{5\omega_p^4}{4\omega^4}\right) d\omega \tag{11}$$

Terms ω_p is peak frequency in rad/s, γ is peak enhancement factor, α is constant that relates to the wind speed and the peak frequency of wave spectrum, g is gravitational acceleration in m/s^2 , and H_s is specific wave height in m. Thus, to generate the irregular ocean waves specific wave height, peak frequency, and peak enhancement factor must be defined in order to resemble the actual ocean environment condition.

3.3 Numerical Simulation

One of the floating structural characteristics is the response of the body to regular waves or widely called response amplitude operators (RAOs) that are proportional to wave amplitude. AQWA can numerically calculate this characteristic by using (12).

$$[x_j] = \{-\omega^2 (\mathbf{M}_s + \mathbf{M}_a) - i\omega \mathbf{C} + \mathbf{K}_{hys}\}^{-1} [F_j] \tag{12}$$

$$A_{jk} = \frac{\rho}{\omega} \int_{S_0} \text{Im}[\phi_{rk}(\vec{X})] n_j dS \tag{13}$$

$$B_{jk} = -\rho \int_{S_0} \text{Re}[\phi_{rk}(\vec{X})] n_j dS \tag{14}$$

Terms x_j is position at j -th wave direction ($j = 1, 6$), \mathbf{M}_s is structural mass matrix, $\mathbf{M}_a = [A_{jk}]$ is hydrodynamic added mass matrix, $\mathbf{C} = [B_{jk}]$ is hydrodynamic damping matrix, ρ is water density, S_0 is mean_wetted surface body, ϕ_{rk} is radiation wave potential by k -th unit amplitude body rigid motion, F_j is total force at j -th wave direction, and \mathbf{K}_{hys} is hydrostatic stiffness matrix. To obtain the structure's displacement within a certain time, hydrodynamic time response in AQWA can be employed with

numerical calculation by using global equation of motion that follows (15).

$$MA = F_t \tag{15}$$

Terms M is the assembled structural and added mass matrix, A is the unknown acceleration vector, and F_t is the total applied force that can be written as (16):

$$F_t = F(t) - c\dot{X}(t) - KX(t) - \int_0^t h(t-\tau)\ddot{X}(\tau)d\tau \tag{16}$$

Terms $F(t)$ is total external force matrix, c is damping matrix including the linear radiation damping effects, K is total stiffness matrix, and h is acceleration impulse function matrix which is defined in (17).

$$h(t) = \frac{2}{\pi} \int_0^\infty B(\omega) \frac{\sin(\omega t)}{\omega} d\omega \tag{17}$$

With $B(\omega)$ is the hydrodynamic damping matrix that is defined in (14). The structural phase (position, velocity, and acceleration) at time t can be obtained from acceleration in (15) by using the iteration process and stage predictor. Once the floating structure moves at the six degrees of motion, both taut and catenary moorings will hold the structure position with their own capability. For taut mooring, the cable type is assumed bears tension without compression with the mooring line tension (T) is defined by (18).

$$T = \begin{cases} k(L - L_0) & \text{if } L > L_0 \\ 0 & \text{if } L \leq L_0 \end{cases} \tag{18}$$

Terms k is mooring line stiffness, L_0 is initial unstretched length, and L is stretched length of the mooring line. The catenary mooring contains more than two different materials with the mooring line's acting force illustrated in Fig. 3.

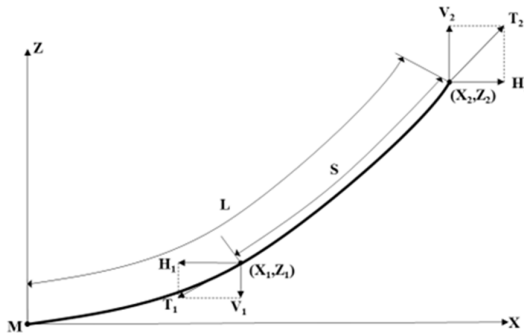


Fig. 3. Force Diagram of Catenary Mooring.

With zero slopes at the contact/attachment point on the sea bed, these equations can be written as (19)-(22).

$$H_2 = EA \sqrt{\left(\frac{T_2}{EA} + 1\right)^2 - \frac{2wZ_2}{EA} - EA} \quad (19)$$

$$X_2 = \frac{H_2}{w} \sinh^{-1}\left(\frac{wL}{H_2}\right) + \frac{H_2 L}{EA} \quad (20)$$

$$V_2 = wL \quad (21)$$

$$T_2 = \sqrt{H_2^2 + V_2^2} \quad (22)$$

Terms EA is the stiffness per unit length, w is the submerged weight per unit length, L is the unstretched length from origin to the attachment point (X_2, Z_2), T is the tension of mooring line, V is the force in the vertical axis, and H is the force in the horizontal axis. For the left-hand end (X_1, Z_1), corresponding equations are expressed in (23)-(27).

$$X_1 = \frac{H_1}{w} \ln\left(\frac{V_2 + T_2}{V_1 + T_1}\right) + \frac{H_1 S}{EA} \quad (23)$$

$$Y_1 = \frac{V_2 + V_1}{T_2 + T_1} S + S \frac{V_2 + V_1}{2EA} \quad (24)$$

$$H_1 = H_2 \quad (25)$$

$$V_1 = V_2 - wS \quad (26)$$

$$T_1 = \sqrt{H_1^2 + V_1^2} \quad (27)$$

Some parameters should be determined for the cable mooring specification, such as length, stiffness, weight per length, and cross-section area. Indubitably, attachment point and anchor position must be convenient with the cable length and water depth.

4 RESULTS AND DISCUSSIONS

The buoy geometry has been developed by using Solidworks with some iterations of shape and dimension. The selected geometry parameters are shown in Table 1. There is also the hydrostatic stability result within Table 1 as the preliminary analysis of the buoy structure. Both metacentric heights in the positive range with a longitudinal height is 0.456 m and a transverse height is 0.456 m. It can be concluded that the buoy structure is in a stable equilibrium. This is strengthened by the position of center of gravity, which is straight vertically to the center of buoyancy.

Table 1. Geometry and Hydrostatic Parameters of Buoy Structure.

Parameter	Value	Unit
Buoy Diameter	2	m
Height	4.75	m
Center of Gravity	$x_g=1.231e-5; y_g=-3.026e-3; z_g=0.125$	m
Mass Moment of Inertia	$I_{xx}=518.86; I_{yy}=519.15; I_{zz}=72.34$	kg.m ²
Draught	1.7	m
Total Applicable Mass	974.376	kg
Volumetric Displacement	0.948	m ³
Cut Water Plane Area	3.136	m ²
Second Moments of Area	$I_{xx}=0.783; I_{yy}=0.783$	m ⁴
Center of Buoyancy	$x_b=1.231e-5; y_b=-3.026e-3; z_b=-0.245$	m
CoG to CoB	0.369	m
Metacentric Heights	$GM_L=0.456; GM_T=0.456$	m

Mesh independence test has been performed within the simulation as the preliminary validation of the numerical calculation by comparing the wave force exciting the buoy structure subjected to the mesh configuration at two buoy motion directions, such as heave and roll. Both motions were selected due to the most critical motion directions in the development of the DVA automation system. Since the buoy geometry is symmetrically in the vertical plane, the roll motion can represent the pitch motion. The mesh independence test result is shown in Fig. 4 and detailed mesh configurations with its residual value are tabulated in Table 2. It can be seen from the heave force that all mesh configurations have a similar trend with a maximum error of 0.254% at the biggest mesh size (configuration F). Thus, the analysis continued to the roll moment, which was quietly visible for the difference between each configuration. Starting from configuration D, with a defeaturing tolerance of 0.04 mm, it has an error value of 0.811%, which is below 2%. Hence, otherwise specified, configuration D is chosen for the simulation to make the simulation task work efficiently.

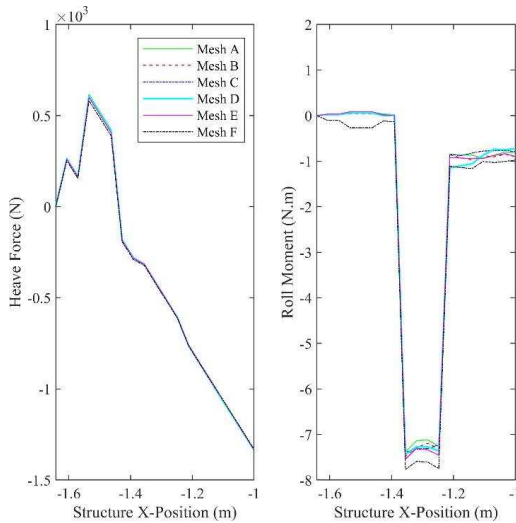


Fig. 4. Mesh Independence Test Result.

Table 2. Mesh Configuration.

Configuration	Defeaturing Tolerance	Total Elements	Roll Moment Residual
Mesh A	0.025 mm	24761	-
Mesh B	0.030 mm	18198	0.032 %
Mesh C	0.035 mm	13039	0.123 %
Mesh D	0.040 mm	10437	0.814 %
Mesh E	0.050 mm	9295	2.241 %
Mesh F	0.060 mm	5095	5.254 %

As stated in the previous section, the simulation is held in the irregular wave condition for the hydrodynamic analysis. It has been performed successfully within the simulation domain, mooring parameters, and wave parameters which are tabulated in Table 3. Wave parameters are determined from the average ocean wave condition in Indonesia with the long-crested waves approach. The wave was developed in the 180° direction as illustrated in Fig. 5. Due to the symmetrical shape of the buoy structure in the vertical plane, there is no significant contribution from the variation of wave directions. Finding result, RAOs of the buoy structure as shown in Fig. 6 for all six buoy motions, shows that the highest amplitude ratio value mostly appeared in the frequency 0.4 Hz. Heave motion has shown a different trend with the stable ratio value of 1 at the range of frequency 0 - 0.5 Hz. It means that the buoy structure still remains on a similar draught corresponding to the sea water level until wave frequency 0.5 Hz. Analysis continued to irregular wave excitation in the 300 s time response subject to three mooring types, such as single-taut, single-line catenary, and four-lines catenary moorings with the buoy displacement result shown in Fig. 7.

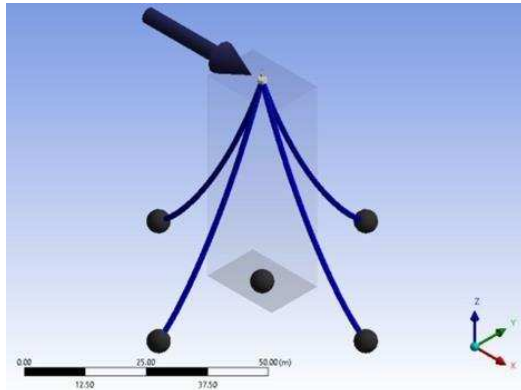


Fig. 5. Wave Direction on Catenary 4-lines Mooring Simulation.

Table 3. Simulation Parameters

Parameter	Value	Unit
Water Depth	50	m
Water Density	1025	kg/m ³
Gravity	9.807	m/s ²
Significant Wave Height	2	m
Gamma	2	-
Peak Frequency	0.2	Hz
<i>Taut Mooring</i>		
Stiffness per Unit Length	2.186e7	N/m
Unstretched Length	48.4	m
<i>Catenary Mooring</i>		
	<i>Chain</i>	<i>Cable Rope</i>
Stiffness	2.186e7	1.055e8
Mass per Unit Length	5.56	4.19
Maximum Tension	1.848e5	7.15e5
Equivalent Diameter	0.016	0.032
Unstretched Length	10	1-line: 28.4 4-lines: 38.31
Catenary Section	Chain-Cable Rope-Chain	
	<i>Anc1:</i> (0;30;-50)	
	<i>Anc2:</i> (30;0;-50)	
	<i>Anc3:</i> (0;-30;-50)	
	<i>Anc4:</i> (-30;0;-50)	
Catenary 4-lines Anchor Position [X;Y;Z]		m

The majority of translational motions (surge, sway, and heave) and rotational motions (roll, pitch, yaw) show that four-lines catenary configuration has the smallest displacement besides the heave motion. This is coherent result since the buoy was held by four attachments with the fairly tight cable length. It has maximum displacement of surge 3.354 m, sway 0.287 m, heave 1.874 m, roll 22.818°, pitch 24.427°, and yaw 54.542°. In the heave motion, the smallest displacement of buoy has been achieved on the single-line catenary mooring, which has a maximum heave displacement of 1.637 m (slightly difference to the four-lines mooring).

Hydrodynamic analysis also considers the cable tension performance of related mooring types. Following that, cable tension of three mooring types were obtained within the simulation and the result was depicted in Fig. 8. The highest cable tension is achieved by single-taut mooring with maximum tension of 166.713 kN, while the

smallest tension appears in the four-lines catenary mooring with a maximum cable tension 32.175 kN. Hereafter, the hydrodynamic analysis result can accomplish mooring type selection for the buoy system.

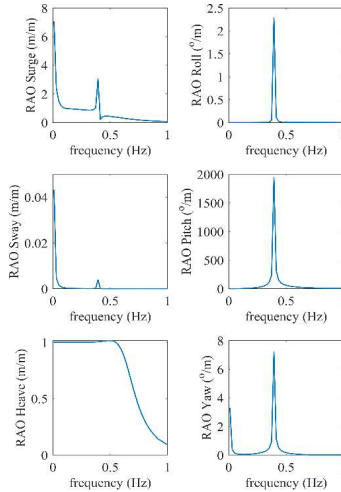


Fig. 6. RAOs of Buoy Structure.

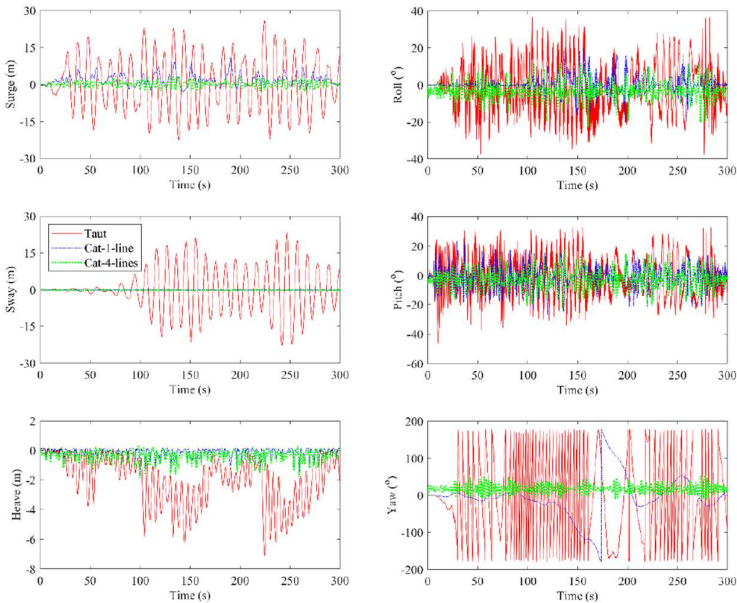


Fig. 7. Buoy Displacement at Six Motions.

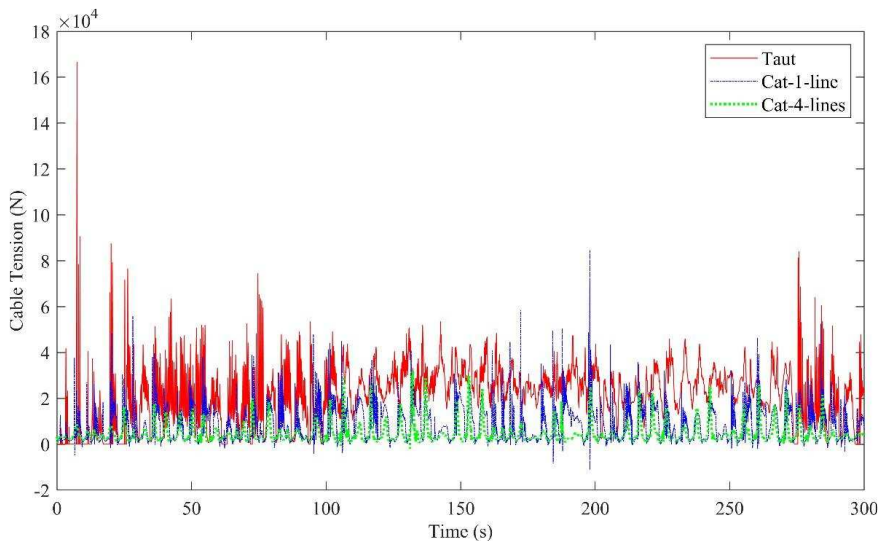


Fig. 8. Cable Tension of Mooring Lines.

5 CONCLUSION AND RECOMMENDATION

Preliminary design of smart buoy with dynamic vibration absorber system has been employed by considering the hydrostatic stability and hydrodynamic characteristic analysis. The lattermost design has demonstrated stable equilibrium in the hydrostatic stability with the metacentric height of 0.456 m. By considering response amplitude operator, displacement of six motions, and cable tension of mooring lines, hydrodynamic characteristic has been evaluated in the irregular wave condition following JONSWAP spectrum with three mooring types, such as single-taut, single-line catenary, and four-lines catenary moorings by using ANSYS AQWA. Findings show that the buoy structure produces a high amplitude ratio of 0.4 Hz, and four-lines catenary mooring delivered a good performance. The maximum buoy displacement for this configuration as follows: surge 3.354 m, sway 0.287 m, heave 1.874 m, roll 22.818°, pitch 24.427°, and yaw 54.542° along 300 s response. It takes a maximum cable tension of 32.175 kN, which is below its maximum specification and less than another mooring configuration.

By examining the result, four-lines catenary mooring type is the most suggested configuration to be applied in the floating structure, particularly for the buoy system. Some consideration must be evaluated for the application, such as production, installation, and maintenance cost of mooring line. Furthermore, this study can be followed by dynamic vibration absorber (DVA) automation system development as the main feature of the communication noise reducer buoy, and an experimental method can be performed to conform to the final buoy design.

Acknowledgments. The authors are grateful to the Research Center for Smart Mechatronics for providing the facility and to the Electronics and Informatics Research Organization – National

Research and Innovation Agency for financial support through Program House: Artificial Intelligence, Big Data, and Computational Technology for Biodiversity and Satellite Imaging No. 1/III.6/HK/2023.

References

1. H. Venkatesan, Ramasamy & Ramesh, Krishnamoorthy & Kishor, Anand & Vedachalam, Narayanaswamy & Atmanand, Ma. (2018). Best Practices for the Ocean Moored Observatories. *Frontiers in Marine Science*. 5. 10.3389/fmars.2018.00469.
2. Milburn, H., Nakamura, A., and Gonzalez, F. (1996). Real-time tsunami reporting from the deep ocean. *Proceedings of the Oceans 96 MTS/IEEE Conference*, 390–394.
3. Sandra L. Castro, Gary A. Wick, Michael Steele, “Validation of satellite sea surface temperature analyses in the Beaufort Sea using UpTempO buoys”, *Remote Sensing of Environment*, Volume 187, 2016, Pages 458- 475, ISSN 0034-4257, <https://doi.org/10.1016/j.rse.2016.10.035>.
4. Juan F. Martínez-Osuna, Francisco J. Ocampo-Torres, Lucía Gutiérrez-Loza, Ernesto Valenzuela, Angel Castro, Rodrigo Alcaraz, Carlos Rodríguez, Luis R. Ulloa, “Coastal buoy data acquisition and telemetry system for monitoring oceanographic and meteorological variables in the Gulf of Mexico”, *Measurement*, Volume 183, 2021, 109841, ISSN 0263-2241, <https://doi.org/10.1016/j.measurement.2021.109841>.
5. R. Hostache, P. Matgen, L. Giustarini, F.N. Teferle, C. Tailliez, J.-F. Iffly, G. Corato, “A drifting GPS buoy for retrieving effective riverbed bathymetry”, *Journal of Hydrology*, Volume 520, 2015, Pages 397-406, ISSN 0022-1694, <https://doi.org/10.1016/j.jhydrol.2014.11.018>.
6. A. Schrott, M. Raab and H. Forster, "The antenna system of a distress buoy for use in a maritime satellite communication system (MARSAT)," in *IEEE Transactions on Antennas and Propagation*, vol. 24, no. 1, pp. 102-105, January 1976, <https://doi.org/10.1109/TAP.1976.1141289>.
7. Mbay, La & Rahmania, Rinny. (2010). Construction of coastal buoy to support aquaculture activities in Seribu islands. *Jurnal Kelautan Nasional*. 5.
8. Schöne, T. & Pandoe, Wahyu & Mudita, Imam & Roemer, Swen & Illigner, J. & Zech, C. & Galas, Roman. (2011). GPS water level measurements for Indonesia's Tsunami Early Warning System. *Natural Hazards and Earth System Sciences – NAT HAZARDS EARTH SYST SCI*. 11. 741-749. <https://doi.org/10.5194/nhess-11- 741-2011>.
9. Jong-In Byun, Seok-Won Choi, Myeong-Han Song, Byung-Uck Chang, Yong-Jae Kim, Ju-Yong Yun, “A large buoy-based radioactivity monitoring system for gamma-ray emitters in surface seawater”, *Applied Radiation and Isotopes*, Volume 162, 2020, 109172, ISSN 0969-8043, <https://doi.org/10.1016/j.apradiso.2020.109172>.
10. Yuji Tomizawa, Masayoshi Toda, “Oscillation Reduction Control for Ocean Environment Monitoring Buoys”, *IFAC Proceedings Volumes*, Volume 43, Issue 20, 2010, Pages 277-282, ISSN 1474-6670, ISBN 9783902661883, <https://doi.org/10.3182/20100915-3-DE-3008.00024>.
11. B.A. Niclasen, K. Simonsen, “Note on wave parameters from moored wave buoys”, *Applied Ocean Research*, Volume 29, Issue 4, 2007, Pages 231-238, ISSN 0141-1187, <https://doi.org/10.1016/j.apor.2008.01.003>.
12. Wang, Xifeng & Ichikawa, Kaoru. (2016). Effect of High-Frequency Sea Waves on Wave Period Retrieval from Radar Altimeter and Buoy Data. *Remote Sensing*. 8. 764. <https://10.3390/rs8090764>.

13. Antony Joseph, Chapter 3 - Lagrangian-Style Surface Current Measurements Through Tracking of Surface Drifters, Editor(s): Antony Joseph, Measuring Ocean Currents, Elsevier, 2014, Pages 93-107. ISBN 9780124159907, <https://doi.org/10.1016/B978-0-12-415990-7.00003-X>.
14. H. Behzad and R. Panahi, "Optimization of bottom-hinged flap-type wave energy converter for a specific wave rose," *Journal of Marine Science and Application*, 16 159–165 (2017). <https://doi.org/10.1007/s11804-017-1405-y>.
15. J. C. Park, C. M. Wang and I. H. Cho, "Hydrodynamic behaviour of floating polygonal compound platforms with wide porous media," *Ocean Engineering*, 265 112672 (2022). <https://doi.org/10.1016/j.oceaneng.2022.112672>.
16. F. Huijs, R. de Bruijn and F. Savenije, "Concept Design Verification of a Semi-submersible Floating Wind Turbine Using Coupled Simulations," *Energy Procedia*, 53 2-12 (2014). <https://doi.org/10.1016/j.egypro.2014.07.210>.
17. Y. I. Chu and C. M. Wang, "Hydrodynamic Response Analysis of Combined Spar Wind Turbine and Fish Cage for Offshore Fish Farms," *International Journal of Structural Stability and Dynamics*, 20 09 (2020). <https://doi.org/10.1142/S0219455420501047>.
18. M. Rajabi and H. Ghassemi, "Hydrodynamic Performance Improvement of Double-Row Floating Breakwaters by Changing the Cross-Sectional Geometry," *Mathematical Problems in Engineering*, 2021 2944466 (2021). <https://doi.org/10.1155/2021/2944466>.
19. S.R. Samei, F. Azarsina and M. A. Ghahferokhi, " Numerical Simulation of Floating Pontoon Breakwater with ANSYS AQWA Software and Validation of the Results with Laboratory Data," *Bulletin de la Société Royale des Sciences de Liège*, 85 1487 - 1499 (2016). <https://doi.org/10.25518/0037-9565.6194>.
20. Y. Junwei, Z. Shaowei, Y. Wencai, X. Yongzhi, and G. Huaining, "Design and Application of Buoy Single Point Mooring System with Electro-Optical-Mechanical (EOM) Cable," *J. Mar. Sci. Eng.* 2020, 8(9), 672; <https://doi.org/10.3390/jmse8090672>.
21. Houmb, O.G. and Overvik, T. (1976), 'Parameterization of wave spectra', *Proceeding of the first Conference on Behaviors of Offshore Structures (BOSS' 76)*, Trondheim, Norway, Vol. 1, pp.144-169. M. P. Brown and K. Austin, *The New Physique* (Publisher Name, Publisher City, 2005), pp. 25–30.

Open Access This chapter is licensed under the terms of the Creative Commons Attribution-NonCommercial 4.0 International License (<http://creativecommons.org/licenses/by-nc/4.0/>), which permits any noncommercial use, sharing, adaptation, distribution and reproduction in any medium or format, as long as you give appropriate credit to the original author(s) and the source, provide a link to the Creative Commons license and indicate if changes were made.

The images or other third party material in this chapter are included in the chapter's Creative Commons license, unless indicated otherwise in a credit line to the material. If material is not included in the chapter's Creative Commons license and your intended use is not permitted by statutory regulation or exceeds the permitted use, you will need to obtain permission directly from the copyright holder.

